LETTERS
PUBLISHED ONLINE: 4 JANUARY 2016 | DOI: 10.1038/NCLIMATE2899
nature climate change

Greenland meltwater storage in firn limited by near-surface ice formation

Horst Machguth[1,2*†], Mike MacFerrin[3], Dirk van As[1], Jason E. Box[1], Charalampos Charalampidis[1,4], William Colgan[1,5], Robert S. Fausto[1], Harro A. J. Meijer[6], Ellen Mosley-Thompson[7] and Roderik S. W. van de Wal[8]

Approximately half of Greenland's current annual mass loss is attributed to runoff from surface melt[1]. At higher elevations, however, melt does not necessarily equal runoff, because meltwater can refreeze in the porous near-surface snow and firn[2]. Two recent studies suggest that all[3] or most[3,4] of Greenland's firn pore space is available for meltwater storage, making the firn an important buffer against contribution to sea level rise for decades to come[3]. Here, we employ *in situ* observations and historical legacy data to demonstrate that surface runoff begins to dominate over meltwater storage well before firn pore space has been completely filled. Our observations frame the recent exceptional melt summers in 2010 and 2012 (refs 5,6), revealing significant changes in firn structure at different elevations caused by successive intensive melt events. In the upper regions (more than ~1,900 m above sea level), firn has undergone substantial densification, while at lower elevations, where melt is most abundant, porous firn has lost most of its capability to retain meltwater. Here, the formation of near-surface ice layers renders deep pore space difficult to access, forcing meltwater to enter an efficient[7] surface discharge system and intensifying ice sheet mass loss earlier than previously suggested[3].

In Greenland's accumulation area, porous firn up to 80 m thick underlies the ice sheet surface[8]. Whereas most of the contemporary firn extent experienced limited melt in the past, recent exceptional melt events now reach the highest parts of the ice sheet[5]. Consequently, the percolation area, where the infiltration of surface meltwater into the firn redistributes mass vertically and horizontally[9], is expanding. It is estimated that, at present, 30–40% of melt is retained in the firn[1,4]. However, direct quantifications are subject to large uncertainties, and understanding feedback mechanisms in Greenland's changing firn is vital to assess and project ice sheet mass balance.

Meltwater percolating in firn can be retained as liquid by capillary forces[10], in firn aquifers[11], or by refreezing in firn pore space, whereby refrozen meltwater forms ice horizons or lenses[12]. If cold content and unfilled pore space are available, refreezing is very efficient for long-term meltwater retention[13] and thus buffers mass loss[2,13]. A recent study[3] postulates two endmember pathways of the uncertainty in calculating this buffer, with meltwater either percolating deep into the firn, eventually consuming all pore space, or aggregating in low-permeability ice layers near the surface that render underlying pore space unavailable to further refreezing. Field data from the years 2007 to 2009 (ref. 14) suggested that the former is more likely, implying that firn will remain an important meltwater buffer in coming decades[3,4] and that substantial runoff from the percolation area starts once all firn pore space is filled[3].

In summer 2012, Greenland experienced the largest observed melt extent on record[5]. Satellite images (Fig. 1 and Supplementary Figs 1 and 2) of the western flank of the ice sheet at 67° N show meltwater runoff channels reached to unprecedented elevations ~300 m above and ~25 km east of the longer term equilibrium line altitude (1,550 m above sea level (a.s.l.); ref. 15), implying that the limits of firn retention had been reached. Here, we employ *in situ* data to characterize the state of the firn in this region and quantify the impact of large melt on the partitioning between advection (that is, surface runoff) and diffusion (that is, percolation) of water. Our data include 26 firn cores drilled primarily along a transect at 67° N in West Greenland (see Methods and Fig. 1). Cores were drilled in spring 2009, 2012, 2013 and 2015, and thus bracket two recent extraordinary melt seasons of 2010 and 2012. Firn temperatures were monitored at one site and a 110 km firn radar transect connects the cores. These recent cores are compared with cores drilled in 1997 and 1998 to assess changes in firn properties over the past ~15 years.

The 2013 cores (Fig. 2) reveal two statistically distinguishable patterns in firn stratigraphy (see Methods), hereafter referred to as 'firn regimes'. At elevations >1,900 m a.s.l. the firn column contains ice lenses whose average thickness and amount decrease with elevation. Active percolation of meltwater takes place in this zone[14], which we accordingly term the 'firn percolation regime'. At 1,840 m a.s.l., a ~5.5-m-thick near-surface ice layer overlies porous firn. The layer is not a local phenomenon and is clearly recognizable in radar profiles (see Methods) where it is continuously traced both locally on a 1 × 1 km radar grid, and regionally from the lowermost appearance of porous firn (~1,680 m a.s.l.) to ~1,870 m a.s.l. (Supplementary Fig. 3). A similar firn stratigraphy is also found in a core drilled 50 km further south, close to the local summer 2012 runoff limit (Fig. 1 and Supplementary Fig. 4). Below,

[1]Geological Survey of Denmark and Greenland GEUS, 1350 København K, Denmark. [2]Arctic Technology Centre ARTEK, Technical University of Denmark, 2800 Kgs. Lyngby, Denmark. [3]Cooperative Institute for Research in Environmental Sciences (CIRES), University of Colorado at Boulder, Boulder, Colorado 80309, USA. [4]Department of Earth Sciences, Uppsala University, 752 36 Uppsala, Sweden. [5]Department of Earth and Space Science and Engineering, York University, Toronto, Ontario M3J 1P3, Canada. [6]Centre for Isotope Research (CIO), Energy and Sustainability Research Institute Groningen (ESRIG), University of Groningen, 9747AG Groningen, The Netherlands. [7]Byrd Polar and Climate Research Center and Department of Geography, The Ohio State University, Columbus, Ohio 43210, USA. [8]Institute for Marine and Atmospheric Research Utrecht (IMAU), University of Utrecht, 3584CC Utrecht, The Netherlands. †Present address: Department of Geography, University of Zurich, 8057 Zurich, Switzerland.
*e-mail: horst.machguth@geo.uzh.ch

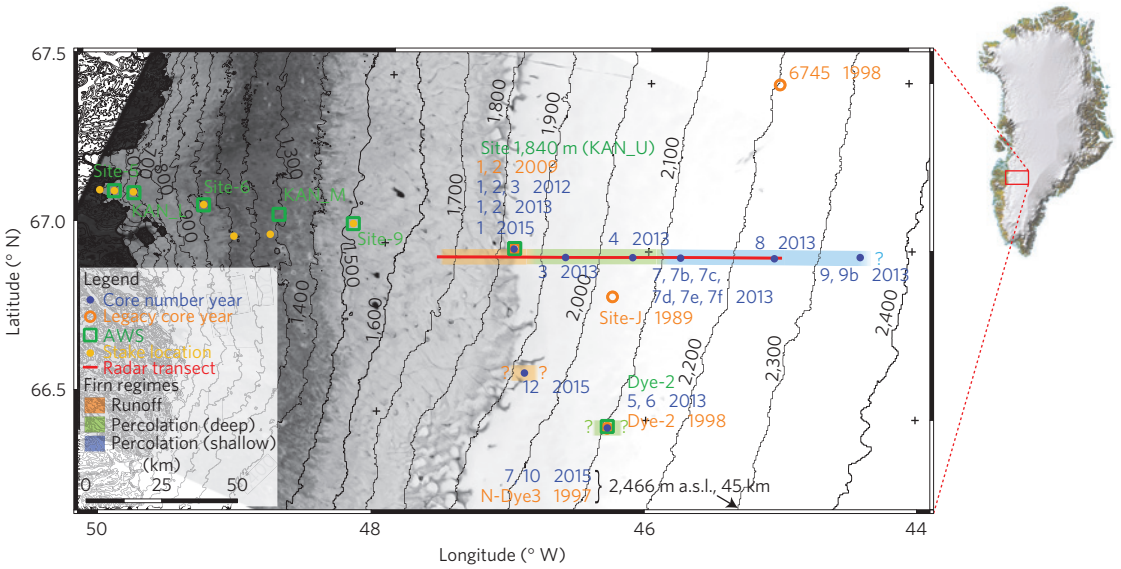

Figure 1 | Map illustrating the firn core sites and main radar transect. Cores collected within our project are in blue; legacy cores are in orange; automatic weather stations are denoted in green. In the background is a panchromatic Landsat 7 image from 16 July 2012, courtesy of USGS/NASA.

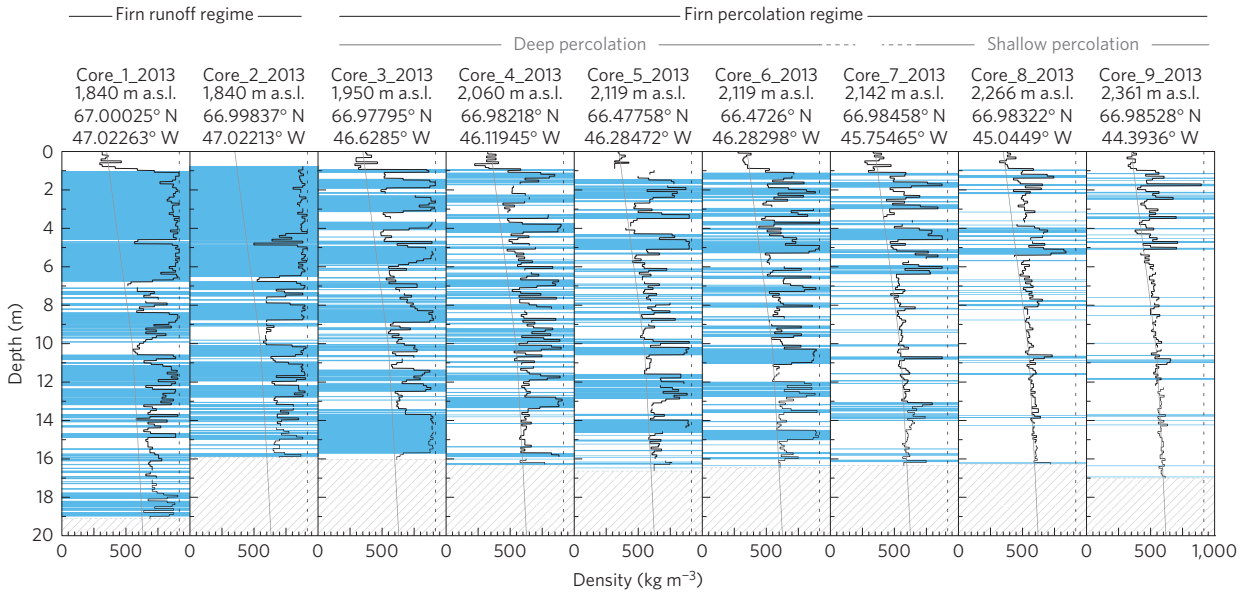

Figure 2 | Stratigraphy of the nine major firn cores drilled in late April to mid May 2013. Ice lenses are in blue and given at 1 cm vertical resolution. Density at 10 cm resolution is in black. The dotted vertical line indicates the density of pure ice (917 kg m^{-3}); the thin inclined line denotes dry firn density according to ref. 8. Dashed areas mark the end of the cores. The association of each core with the suggested firn regimes is indicated at the top.

we show that meltwater in the zone of thick near-surface ice layers is dominated by advection, rather than by diffusion, and we thus apply the term 'firn runoff regime'.

Comparing 2013 and 2015 firn density profiles to analogous 2012, 2009, 1998 and 1997 profiles reveals characteristics in meltwater percolation and their changes over time (Fig. 3). Whereas the 2012 and 2009 data represent the state immediately before the extraordinary melt summers of 2012 and 2010, respectively, the 1997/1998 cores[16] were drilled early in the recent period of strong warming in West Greenland that started in the mid-1990s (refs 1,17). Comparing 1997/1998 and 2013/2015 cores located in the upper part of the percolation regime we find, at 2,466 m a.s.l., a mean density increase of 46 kg m^{-3} in the top 7 m of firn (1 to 8 m depth) and 15 kg m^{-3} between 8 and 16 m depth; at 2,250 m a.s.l. density increased by ~100 kg m^{-3} (1 to 8 m depth) and 18 kg m^{-3} below (8 to 12.6 m core bottom depth). Surface meltwater generated in the recent summers refroze as ice lenses in the upper half of the cores. The ice lenses are thin and sparse, indicating limited melt, all of which the firn is capable of retaining locally. Comparing 1998 and 2013 cores in the lower part of the percolation firn regime (2,120 m a.s.l.) indicates an increase in mean density of ~142 kg m^{-3} in the top 7 m of firn and ~102 kg m^{-3} increase at 8 to 16 m depth. Density around the 1998 surface layer (now at 9.5 ± 1 m depth) has increased more than would result from dry firn compaction alone (compare Fig. 2), indicating that post-1998 ice lenses are now present in pre-1998 firn. We interpret this as evidence of deep (>10 m) meltwater percolation[14] that has modified firn stratigraphy over the entire depth of the 2013 cores (Fig. 3). Limited amounts of subsurface runoff cannot be ruled out where deep percolation prevails[11,14,18].

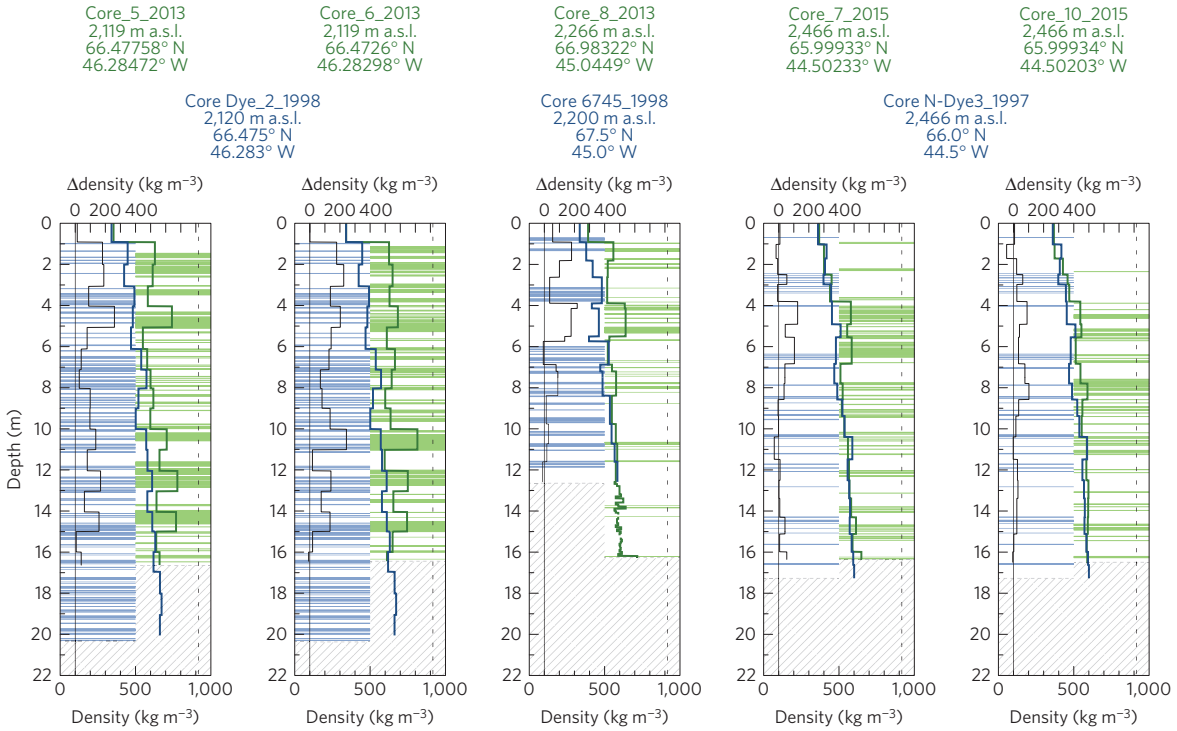

Figure 3 | Changes in firn density from 1997 or 1998 (ref. 16) to 2013 or 2015. Measured firn densities are denoted with blue (1997 or 1998) and green lines (2013 or 2015), and the change in firn density is indicated by the black lines. Ice lenses are shown as pale blue (1997, 1998) and pale green (2013, 2015) horizontal lines. Note that core_8_2013 and core_6745_1998 are separated by ~50 km horizontally and a ~60 m elevation difference. 1998 and 1997 coordinates are of limited accuracy. Legacy core elevations were derived using available coordinates[16] and a recent DEM (ref. 26). Potential vertical displacements of drill sites since 1998 are insignificant owing to low surface velocities (at Dye-2 ~30 m yr^{-1}) and very low surface slopes.

Pronounced temporal changes in the firn towards a runoff regime are illustrated using cores from 2009 to 2012 at 1,840 m.a.s.l (Supplementary Fig. 4). The date of initiation of the thick ice layers observed in 2012 cannot be established, but the two 2009 shallow cores indicate that the uppermost ~2.5 m of the firn contained a small amount of ice (~14%) in 2009. After 2009, and before spring 2012, near-surface meltwater storage exceeded the creation of new pore space, shown by the ice content in the uppermost 2.5 m of firn increasing to 60%. Pore space located below the depth of the shallow 2009 cores was probably filled as well, but in 2012 the firn below the bottom of the ice layers (~7 m depth, Fig. 2) is still of similar appearance to the firn percolation regime. This indicates that deep percolation prevailed before the build-up of the near-surface ice layers, and that during the transition from percolation to runoff regime the traces of the former were preserved at depth.

Comparing stratigraphy and density profiles from May 2012 to 2013 in the firn runoff regime (Supplementary Fig. 4) shows that 0.92 ± 0.1 m water equivalent (w.e.) of surface meltwater was generated in summer 2012, but only 0.23 ± 0.1 m w.e. refroze within the subsurface, forcing 0.69 ± 0.15 m w.e. (or $75 \pm 15\%$) of the total melt to exit the location as runoff (see Methods). Hereafter the term runoff refers to water that is not retained locally and enters an efficient[7] surface discharge system (Supplementary Fig. 1). The core comparison also indicates that in summer 2012, refreezing filled firn layers down to ~5 m depth (Supplementary Fig. 4). Temperatures measured to 15 m depth confirm percolation to 5 m depth in September (Supplementary Fig. 5). Neither the core comparison nor the firn temperature data show signs of significant 2012 percolation below the base of the thick ice layer. Firn underlying the ~5.5 m thick ice layer is effectively isolated from subsequent percolation, even from extraordinary events such as in 2012. Now difficult to access, this 'relict' pore space below the thick ice layer comprises, at the 1,840 m site, $32 \pm 10\%$ of the total pore space that would exist in a hypothetical situation with dry firn compaction alone (see Methods).

The low permeability of the thick near-surface ice layers is corroborated by a network of summer 2012 surface meltwater channels (Fig. 1 and Supplementary Fig. 1), extending over the entire zone of the firn runoff regime up to an unprecedented elevation of ~1,850 m a.s.l. (see Methods and Supplementary Fig. 2). Satellite imagery and the radar transect document that 200-m-wide braided supraglacial rivers flow atop the ice layers (Supplementary Figs 1 and 3), providing further evidence that underlying relict pore space is effectively isolated in 2012. Using elevation profiles of surface melt and hypsometry, we quantify, on a regional scale, how the transition from percolation to firn runoff regime increases ice sheet discharge (see Methods). The calculation indicates that $11 \pm 4\%$ of total regional runoff of the 2012 melt season originated from the elevation range of the firn runoff regime. We thus conclude that changing firn regimes played a significant role in extraordinary proglacial discharge observed in the region[7].

On the basis of *in situ* data, we have documented a pathway of firn response to recent warming. At higher elevations, firn density and ice lens frequency have increased owing to active meltwater retention, including processes of deep percolation[3,14]. At lower elevations, where melt is most abundant, thick near-surface ice layers have formed that limit deep percolation, render existing deep pore space difficult to access and force most meltwater to migrate along the surface. In contrast to suggestions arising from previous research[3], we find that complete pore space filling is not a prerequisite to intensive surface runoff. Instead, the latter occurs as soon as firn conditions correspond approximately to the lower endmember scenario of firn buffering capacity outlined in ref. 3 (that is, only the uppermost 10 m of firn pore space are available to retain melt), with the implication of shortening the estimated timing of sea level rise contribution from the percolation area.

Our conclusions refer to the impact of near-surface ice layers under the extraordinary melt conditions of summer 2012; partitioning of surface migration and percolation could be different during gentle melt seasons. Comparing 2013 and 2015 stratigraphy at the 1,840 m site (Supplementary Fig. 4 and Methods) indicates that melt generated during the moderate melt seasons of 2013 and 2014 has partly accreted as superimposed ice on top of the ice layer. Melt rivers originate at high elevations in both summers (Supplementary Fig. 2), providing further evidence that even limited quantities of water now mainly migrated along the surface.

Our findings relate to one transect and do not allow interference on the impact of changing firn regimes at the ice sheet scale. However, similar changes in firn structure are observed in the Canadian Arctic[19–21]. A study of Greenland's percolation area 250 km north of our study site also indicates ice formation in the near surface[22]. Common to these sites and our study region is the onset of substantial melt under relatively cold and dry climatological conditions. As these are typical for most of Greenland's percolation area, it seems unlikely that documented changes, and their related impact, are solely of local origin.

Provided persistent climate warming[23], the firn runoff regime will probably migrate to higher elevations[24]. Owing to amplifying feedback processes, surface runoff from the zone of thick near-surface ice layers is anticipated to increase beyond its 2012 contribution ($11 \pm 4\%$ of total regional runoff). First, the ice sheet becomes flatter as elevation increases, exposing greater areas to runoff given a step change in the upper boundary of the firn runoff regime. Second, the related emergence of slush fields and runoff channels decreases surface albedo, creating additional melt in these newly saturated regions[25]. The combination of these factors provides firn transition with powerful leverage on Greenland's future mass balance and contribution to sea level rise.

Methods

Methods and any associated references are available in the online version of the paper.

Received 7 April 2015; accepted 17 November 2015; published online 4 January 2016

References

1. van den Broeke, M. *et al.* Partitioning recent Greenland mass loss. *Science* **326,** 984–986 (2009).
2. Pfeffer, W., Meier, M. & Illangasekare, T. H. Retention of Greenland runoff by refreezing: implications for projected future sea level change. *J. Geophys. Res.* **96,** 22117–22124 (1991).
3. Harper, J., Humphrey, N., Pfeffer, W. T., Brown, J. & Fettweis, X. Greenland ice-sheet contribution to sea-level rise buffered by meltwater storage in firn. *Nature* **491,** 240–243 (2012).
4. vanAngelen, J. H., Lenaerts, J. T. M., van den Broeke, M. R., Fettweis, X. & van Meijgaard, E. Rapid loss of firn pore space accelerates 21st century Greenland mass loss. *Geophys. Res. Lett.* **40,** 2109–2113 (2013).
5. Nghiem, S. V. *et al.* The extreme melt across the Greenland ice sheet in 2012. *Geophys. Res. Lett.* **39,** L20502 (2012).
6. van As, D. *et al.* Large surface meltwater discharge from the Kangerlussuaq sector of the Greenland ice sheet during the record-warm year 2010 explained by detailed energy balance observations. *Cryosphere* **6,** 199–209 (2012).
7. Smith, L. C. *et al.* Efficient meltwater drainage through supraglacial streams and rivers on the southwest Greenland ice sheet. *Proc. Natl Acad. Sci. USA* **112,** 1001–1006 (2015).
8. Herron, M. & Langway, J. C. Firn densification: an empirical model. *J. Glaciol.* **25,** 373–385 (1980).
9. Brown, J., Harper, J., Pfeffer, W., Humphrey, N. F. & Bradford, J. High resolution study of layering within the percolation and soaked facies of the Greenland ice sheet. *Ann. Glaciol.* **52,** 35–41 (2011).
10. Colbeck, S. C. A study of glacier flow for an open-pit mine: an exercise in applied glaciology. *J. Glaciol.* **13,** 401–414 (1974).
11. Forster, R. R. *et al.* Extensive liquid meltwater storage in firn within the Greenland ice sheet. *Nature Geosci.* **7,** 95–98 (2013).
12. Benson, C. S. *Stratigraphic Studies in the Snow and Firn of the Greenland Ice Sheet* Res. Rep. 70, reprint (US Army Corps of Engineers, Snow, Ice and Permafrost Research Establishment, 1996).
13. Pfeffer, W. & Humphrey, N. F. Formation of ice layers by infiltration and refreezing of meltwater. *Ann. Glaciol.* **26,** 83–91 (1998).
14. Humphrey, N. F., Harper, J. T. & Pfeffer, W. T. Thermal tracking of meltwater retention in Greenland's accumulation area. *J. Geophys. Res.* **117,** F01010 (2012).
15. Van de Wal, R. S. W. *et al.* Twenty-one years of mass balance observations along the K-transect, West Greenland. *Earth Syst. Sci. Data* **4,** 31–35 (2012).
16. Mosley-Thompson, E. *et al.* Local to regional-scale variability of annual net accumulation on the Greenland ice sheet from PARCA cores. *J. Geophys. Res.* **106,** 33839–33851 (2001).
17. Tedesco, M. *et al.* Evidence and analysis of 2012 Greenland records from spaceborne observations, a regional climate model and reanalysis data. *Cryosphere* **7,** 615–630 (2013).
18. Koenig, L. S., Miège, C., Forster, R. R. & Brucker, L. Initial *in situ* measurements of perennial meltwater storage in the Greenland firn aquifer. *Geophys. Res. Lett.* **41,** 81–85 (2014).
19. Bezeau, P., Sharp, M., Burgess, D. & Gascon, G. Firn profile changes in response to extreme 21st-century melting at Devon Ice Cap, Nunavut, Canada. *J. Glaciol.* **59,** 981–991 (2013).
20. Zdanowicz, C. *et al.* Summer melt rates on Penny Ice Cap, Baffin Island: past and recent trends and implications for regional climate. *J. Geophys. Res.* **117,** F02006 (2012).
21. Gascon, G., Sharp, M. J., Burgess, D. O., Bezeau, P. & Bush, A. Changes in accumulation area firn stratigraphy and meltwater flow during a period of climate warming, Devon Ice Cap, Nunavut, Canada. *J. Geophys. Res.* **118,** 2380–2391 (2013).
22. de la Peña, S. *et al.* Changes in the firn structure of the western Greenland Ice Sheet caused by recent warming. *Cryosphere* **9,** 1203–1211 (2015).
23. IPCC *Climate Change 2013: The Physical Science Basis* (eds Stocker, T. F. *et al.*) (Cambridge Univ. Press, 2013).
24. McGrath, D., Colgan, W., Bayou, N., Muto, A. & Steffen, K. Recent warming at summit, Greenland: global context and implications. *Geophys. Res. Lett.* **40,** 2091–2096 (2013).
25. Liang, Y. *et al.* A decadal investigation of supraglacial lakes in West Greenland using a fully automatic detection and tracking algorithm. *Remote Sens. Environ.* **123,** 127–138 (2012).
26. Howat, I. M., Negrete, A. & Smith, B. E. The Greenland Ice Mapping Project (GIMP) land classification and surface elevation data sets. *Cryosphere* **8,** 1509–1518 (2014).

Acknowledgements

This work is supported by the US National Aeronautics and Space Administration (NASA) Grant no. NNX10AR76G, 'Comprehensive Assessment of Ice Sheet Contributions to Sea Level Based on Integrated Remote Sensing Observations', by the Greenland Analogue Project (GAP), funded by Svensk Kärnbränslehantering AB, Sweden, Posiva Oy, Finland, and NWMO, Canada, the Refreeze Project funded by GEUS, the RETAIN project, funded by the Danish Council for Independent research (Grant no. 4002-00234) and the Programme for Monitoring of the Greenland Ice Sheet (PROMICE), funded by The Danish Energy Agency DANCEA programme. Collection and analyses of the legacy cores was supported by NASA's PARCA Program. The K-transect programme has been funded by Utrecht University, the Netherlands Polar Program of NWO/ALW and a Spinoza grant. This publication is contribution number 62 of the Nordic Centre of Excellence SVALI, 'Stability and Variations of Arctic Land Ice', funded by the Nordic Top-level Research Initiative (TRI). The authors acknowledge field assistance by K. Alley, A. Crawford, S. Doyle, M. Eijkelboom, S. Grigsby, D. Hill, A. Heilig, A. Hubbard, K. Lindbäck, R. Petterson and M. Stevens as well as logistical contributions from W. Abdalati, R. Bauer, A. Hubbard and T. Scambos. Satellite imagery in Supplementary Fig. 1 is subject to copyright by European Space Imaging/DigitalGlobe.

Author contributions

H.M. conceived the study; M.M., D.v.A. and H.M. collaboratively designed and planned the field campaigns in which M.M., H.M., D.v.A., C.C. and W.C. participated; H.M., M.M., D.v.A., J.E.B., C.C., W.C., R.S.F. and E.M.-T. performed the data analysis; E.M.-T., R.S.W.v.d.W. and H.A.J.M. prepared and provided additional data. H.M. and M.M. wrote the manuscript; all authors continuously discussed the results and developed the analysis further.

Additional information

Supplementary information is available in the online version of the paper. Reprints and permissions information is available online at www.nature.com/reprints. Correspondence and requests for materials should be addressed to H.M.

Competing financial interests

The authors declare no competing financial interests.

Methods

Field investigations. In April 2009, two 3.5-m-depth cores were obtained at 1,840 m a.s.l. (Fig. 1 and Supplementary Fig. 1). At this site in early May 2012, three 10.5 m cores were obtained, firn temperature strings were installed (three to 10 m and one to 15 m depth) and a 1 × 1 km firn radar grid was recorded. Between 22 April and 22 May 2013, cores were extracted in 100 m elevation intervals between 1,840 and 2,360 m a.s.l. Nine of the fifteen cores were drilled to depths between 16 and 19 m. For all cores, stratigraphy and density were sampled at 1 and 10 cm resolution, respectively. A 110 km radar profile connects all cores of the transect and extends down to 1,660 m a.s.l. One core at 1,840 m a.s.l., one at 1,927 m a.s.l. and two cores at 2,466 m a.s.l., all drilled in May 2015, are also used here.

Relating core stratigraphy to ground-penetrating radar (GPR) data. A Malå 800 MHz shielded GPR Rx/Tx antenna was towed behind a snowmobile, recording traces every 0.5 s at a mean speed of 2.84 m s^{-1}. A total of 2,024 samples were recorded at 0.10 ns intervals within each trace, for a total approximate depth of 20.5 m. Latitude, longitude and elevation were recorded with a Trimble 5700 differential GPS (Global Positioning System) at 1 Hz. After preprocessing, GPR traces were resampled to 1.5 m spacing and merged into a single transect. Ice lenses were identified using a local moving window to identify thick regions of refrozen ice with low signal variances. Additional processing details are provided in the Supplementary Information.

Comparison between radar and core stratigraphy confirms that the near-surface ice layer is continuous from ∼1,680 m a.s.l. to ∼1,870 m a.s.l. (Supplementary Fig. 3). We define the lower limit as the first appearance of underlying firn; and use an approximate definition for the upper limit where the near-surface layer separates into an upper and a lower ice horizon. The firn cores (Fig. 2) also confirm the separation into a sequence of thinner lenses.

Statistically distinguishing firn regimes. We quantify the two firn regimes by investigating the change in available pore space p_t with depth h. We apply the null hypothesis (Student's t-test), that the calculated slopes using the least-squares method of $p_t(h)$ versus depth for all nine 2013 cores are similar. The calculated slopes between the cores in the firn runoff regime are significantly ($p < 1\%$) different from all of the other cores but not from each other ($p = 28\%$). Cores in the percolation regime are not significantly different from each other ($8\% < p < 92\%$).

Summer 2012 mass balance and retention at 1,840 m a.s.l. At 1,840 m a.s.l. (Supplementary Fig. 1) cores were obtained at Sites A and B (∼250 m separation). At Site A core_1_2012, core_2_2012 and core_1_2013 were drilled within a ∼50 m radius; core_3_2012 and core_2_2013 were drilled at a ∼50 m horizontal displacement at Site B, compensating for the ice movement (∼50 m yr^{-1}).

Cores from Sites A and B are grouped in three pairs of repeat cores (Supplementary Fig. 4); for Site A the pairs are core_1_2012/core_1_2013, and core_2_2012/core_1_2013, and for Site B core_3_2012/core_2_2013. A visual comparison of the 2012 cores reveals distinct stratigraphic similarities. Evaluating changes from 2012 to 2013 indicates that firn density shallower than ∼5.2 m increased substantially while below, the characteristic sequence of ice lenses and the density profile remained essentially constant. Depth values hereafter refer to the spring 2013 vertical coordinate system (Supplementary Fig. 4). Changes shallower than 5.2 m are attributed to the in-filling of firn pore space by infiltration and refreezing of meltwater. A pronounced refreezing event is documented by the firn temperature string data (Supplementary Fig. 5 and Supplementary Discussion).

The unchanged lower sections of the density profiles below 5.2 m depth are used to align the pairs of cores using linear regression between the 2012 and 2013 profiles. The two density profiles in each pair of cores are displaced in 1 cm intervals and for each step the regression coefficient of the two profiles is calculated. The displacement for which correlation is at maximum is applied to align the pairs of cores (Supplementary Fig. 4). The aligned profiles are used to calculate the change in density $\Delta\rho$ over the depth range where the 2012 and 2013 profiles overlap. The onset of the ice layer (marked with $EOMS_{2012}$ in Supplementary Fig. 4) is defined as the 2012 end of melt season (EOMS) surface.

Ablation is assumed equal to meltwater production calculated from surface height lowering between spring 2012 and $EOMS_{2012}$. Meltwater retention in 2012 is derived from integrating $\Delta\rho$ below $EOMS_{2012}$. Annual ablation (−0.99, −0.93 and −0.83 m w.e.) and retention (0.27, 0.29 and 0.14 m w.e.) values agree within 0.13 m w.e. among the three pairs. Ablation values are in good agreement to two independent measurements of ablation (−1.00 and −0.91 m w.e., see Supplementary Discussion).

Changes in firn stratigraphy from spring 2013 to spring 2015 at 1,840 m a.s.l. Using the same approach as described above, core_1_2015, drilled in May 2015 at the 1,840 m site, is aligned to core_1_2013 and core_2_2013 (Supplementary Fig. 4). Both pairs of cores indicate accretion of ice on top of the thick ice lenses. With respect to the $EOMS_{2012}$ reference horizon, accretion amounts to 0.49 m (core_1_2013/core_1_2015) or 0.63 m of ice (core_2_2013/core_1_2015). Integrating $\Delta\rho$ over the depth ranges of accreted ice yields 0.20 and 0.31 m w.e. Integrating $\Delta\rho$ below $EOMS_{2012}$ yields also positive values (0.19 m w.e. and 0.1 m w.e). To isolate the effect of meltwater percolation and refreezing from the influence of natural firn compaction, the above values need to be reduced by roughly 0.01 m w.e. (for the depth range of accreted ice) and 0.06 m.w.e. (entire depth range below $EOMS_{2012}$). Percolation and refreezing thus seem more active on top of the thick ice layers, as opposed to below. All calculated numbers, however, are subject to considerable uncertainty as the core comparison is hampered by the 2015 sample consisting of only one core.

Maximum elevation extent of supraglacial rivers, 1985–2014. We consider supraglacial rivers to be unambiguous expressions of surface runoff. Melt river maximum elevation (E_{max}) extent for the time period 1985 to present is mapped in all 78 available Landsat images between 15 July and 31 August that cover the area between the 1,840 m site and the ice sheet margin. E_{max} is defined as the average elevation of the five highest river heads (see Supplementary Discussion) in a 25-km-wide interval north and south of the radar transect (Fig. 1). The transect is linearly projected to the ice margin from its lower (1,660 m a.s.l.) limit. Where more than one image per year exists, the one showing the highest melt river extent was considered (Supplementary Fig. 2). As outlined in Supplementary Discussion, we consider the Landsat analysis to reliably indicate that the melt river extent of the 2012 melt season stands out compared with all other years (see also refs 5,17).

Contribution of 2012 firn-area runoff to total meltwater discharge. The contribution of the firn area to total runoff in summer 2012 is calculated along the K-transect, spanning an elevation range from the ice margin at 300 m a.s.l. to 2,200 m a.s.l. The approach, outlined in the following, avoids ambiguous delineations of ice sheet meltwater catchments[27] and provides a regional-scale estimate. The computation requires knowledge of the elevation profiles of surface melt and hypsometry as well as the fractions of retained meltwater at the different elevations. The calculation incorporates a Monte Carlo framework to assess uncertainty.

First, The hypsometry along the K-transect is calculated over a 10 km width, perpendicular to the K-transect, in 100 m elevation bins over the 300–2,200 m a.s.l. range using the 90 m horizontal resolution GIMP DEM (ref. 26). The transect length per elevation interval is then derived from area per elevation interval and width and expressed as a fraction of mean transect length. The derivative of the hypsometry is finally approximated using a linear regression ($r^2 = 0.884$). See Supplementary Fig. 6.

Second, The elevation profile of ablation in the 2012 melt season is calculated on the basis of *in situ* measurements of annual surface mass balance along the K-transect[6,15], and by means of firn core analysis (1,840 m site, as outlined above). The latter allows retrieval of ablation from spring to autumn 2012. To isolate summer ablation from measured annual surface mass balance, the water equivalent of the snow cover that built up over the time period August 2011 to the onset of melt in spring 2012 is subtracted. Direct measurements of snow water equivalent at 1,840 m a.s.l. indicated a 2012 pre-melt (early May) snow cover of 0.26 m w.e. Snow thickness measured at 1,010 m a.s.l. (Site-6, Fig. 1) is generally low (0.18 m on average from 2003 to 2015), and at Site-5 (490 m a.s.l.) snow is rarely present, corroborating limited accumulation at low elevations[6,15]. Hence, all annual mass balance values from >800 m a.s.l. were adjusted by $c = -0.25$ m w.e. so the values reflect 2012 melt season ablation (Supplementary Fig. 6). As shown in Supplementary Fig. 6, melt is then approximated as a linear function of elevation ($r^2 = 0.947$). Calculated melt is assumed the only source of water. Evaporation also modifies the surface water balance; however, the impact of rainfall and evaporation on water availability at the surface is small[6] and of opposite signs and thus the two processes are neglected.

Third, The firn meltwater retention is quantified by assigning fractions of retained meltwater (R_z) for three characteristic elevation zones (Supplementary Fig. 6). Here a 'zone' refers to elevation intervals and 'area' refers to orographic units. For the elevation below the thick near-surface ice layers ($< z_l = 1{,}680$ m a.s.l.) retention can be neglected[7]. For the ice layer zone (z_l to $z_t = 1{,}870$ m a.s.l.) R_z is assumed to linearly increase from $R_{zl} = 0$ to $R_{1840\,m} = 0.25$, whereas the latter value refers to R_z measured at 1,840 m in core data. No measurements of R_z are available for the area between z_t and an elevation z_m (2,100 m a.s.l.) where all melt is assumed to be retained. A linear increase of R_z from $R_{1840\,m} = 0.25$ to $R_{zm} = 1$ is assumed. The assumption of a linear increase of retention is based on the continuous decrease of ice layer thickness with elevation (Supplementary Fig. 3).

The linear regressions of hypsometry and melt are multiplied to weigh melt with normalized transect length at any given elevation. Integrations over the three elevation intervals of characteristic meltwater retention (300 to 1,680 m a.s.l., 1,680 to 1,870 m a.s.l. and 1,870 m a.s.l. to 2,100 m a.s.l.), and multiplication with the respective $1–R_z$ yield runoff from the three elevation zones.

Overall uncertainty in runoff contributions is computed by embedding the calculation in a Monte Carlo framework according to ref. 28, repeated 5,000 times while the parameters c, z_l, z_t, z_m and $R_{1840\,m}$ are simultaneously varied according to their expected uncertainties (Supplementary Table 1) to account for interaction of individual parameter uncertainties. Uncertainty in the two linear regressions is

quantified as the standard error of the regression slopes. Before each run the parameters are modified according to $k_m = k + \xi\sigma_k$, where ξ is a normally distributed random number whose values are centred at 0 with a standard deviation of 1, k stands for any of the parameters listed above and k_m is the modified parameter value. For each parameter k a new value of ξ is generated; that is, uncertainties σ_k are considered independent.

In each run the modified parameters c and $R_{1840\,m}$ are tested for validity. If c becomes negative its value is set to 0. Whenever the runoff limit z_m lies above the elevation of zero melt z_{no_melt} then z_m is lowered to z_{no_melt}. To account for the observation that melt was abundant in summer 2012 to high elevations, all runs where z_{no_melt} falls below an arbitrarily chosen elevation of 2,100 m a.s.l. are discarded. Sixty-nine per cent of all runs pass this evaluation. Supplementary Table 1 lists the contribution to total runoff from each elevation interval as well as the calculated uncertainties (one standard deviation).

Fraction of relict pore space. At the 1,840 m site the fraction f_r of transient (relic) pore space p_t in the firn column is quantified by comparing the measured transient firn density profiles $\rho_t(h)$ to a reference dry firn profile $\rho_{HL}(h)$ (Supplementary Fig. 7). The latter is calculated according to ref. 8, based on mean annual air temperature (corrected for recent warming) and precipitation, assuming no melt. The total pore space available for melt storage is derived as $p_{HL} = \int_{h_s}^{h_{pc}} \rho_i - \rho_{HL}\,dh$, where h_{pc} and h_s are the pore close-off depth and the bottom of the snow pack, respectively, and ρ_i is the mean density of all 0.1 m core fractions consisting only of ice ($873 \pm 25\,kg\,m^{-3}$). Subsequently, p_t is calculated as $p_t = \int_{h_s}^{h_{pc}} \rho_i - \rho_t\,dh$ and $f_r = p_t / p_{HL}$. The above calculations require knowing $\rho_t(h)$ below the bottom depth h_m of the firn core. On the basis of data from nearby Site-J (ref. 29), we here assume that f_r in between the bottom depth h_l of the thick ice layers and h_m is representative for the unmeasured depth range h_m to h_{pc} ($h_{pc} = 54$ m according to $\rho_{HL}(z)$ for a pore close-off density of $830\,kg\,m^{-3}$). The entire calculation is embedded in a Monte Carlo framework to assess overall uncertainty (Supplementary Table 2). Full details on the calculation of relict pore space fraction are provided in the Supplementary Information.

Data availability. The utilized legacy core data are available at http://research.bpcrc.osu.edu/Icecore/data.

References

27. Lindbäck, K. *et al.* Subglacial water drainage, storage, and piracy beneath the Greenland ice sheet. *Geophys. Res. Lett.* **42,** 7606–7614 (2015).
28. Machguth, H., Purves, R. S., Oerlemans, J., Hölzle, M. & Paul, F. Exploring uncertainty in glacier mass balance modelling with Monte Carlo simulation. *Cryosphere* **2,** 191–204 (2008).
29. Kameda, T. *et al.* Melt features in ice cores from Site J, southern Greenland: some implications for summer climate since AD 1550. *Ann. Glaciol.* **21,** 51–58 (1995).